Electroweak Radiative Corrections to Higgs Production via Vector Boson Fusion using Soft-Collinear Effective Theory

Andreas Fuhrer, Aneesh V. Manohar, and Wouter J. Waalewijn

Department of Physics, University of California at San Diego, La Jolla, CA 92093

Soft-collinear effective theory (SCET) is applied to compute electroweak radiative corrections to Higgs production via gauge boson fusion, $qq \to qqH$. There are several novel features which make this process an interesting application of SCET: The amplitude is proportional to the Higgs vacuum expectation value (VEV), and so is not a gauge singlet amplitude. Standard resummation methods require a gauge singlet operator and do not apply here. The SCET analysis requires operators with both collinear and soft external fields, with the Higgs VEV being described by an external soft ϕ field. There is a scalar soft-collinear transition operator in the SCET Lagrangian which contributes to the scattering amplitude, and is derived here.

PACS numbers: 12.15.Lk, 12.38.Cy, 14.80.Bn

I. INTRODUCTION

High energy scattering processes at partonic center-of-mass energy $\sqrt{\hat{s}}$ have large radiative electroweak corrections due to the presence of $\alpha^n \log^{2n} \hat{s}/M_Z^2$ terms at n^{th} order in perturbation theory, which lead to a breakdown of fixed-order perturbation theory for large values of $\hat{s}$. These large radiative corrections can be systematically computed by various resummation methods [1]. One such method uses Soft-Collinear Effective Theory (SCET) [2–5], summing the large logarithms by the renormalization group evolution in the effective theory. This effective field theory (EFT) approach for spontaneously broken gauge theories such as the $SU(2) \times U(1)$ electroweak theory was developed in Refs. [6–10]. The purely electroweak corrections at LHC energies are significant (e.g. the electroweak corrections to transverse W pair production are 37% at $\sqrt{\hat{s}} = 2$ TeV) and need to be included to get reliable cross-section predictions.

In this paper, we apply effective theory methods to study electroweak radiative corrections to an important LHC process, Higgs production via vector boson fusion (VBF). QCD corrections to the VBF process have been calculated at next-to-leading order (NLO) for the inclusive cross section in Ref. [11] and for the differential cross section in Refs. [12–14]. The gluon-induced contribution at next-to-next-to-leading order (NNLO) was determined in Ref. [15] and the structure-function approach was employed in Refs. [16, 17] to get an accurate approximation to the full NNLO QCD corrections. The NLO electroweak corrections were determined in Refs. [18, 19], which are comparable in size to the QCD corrections and thus numerically important. The EFT method provides additional insight into the form of the radiative corrections. The computation has some interesting field theory features which are discussed below.

The basic diagram is shown in Fig. 1. We will compute the radiative corrections to this process in the hard-scattering regime, where the outgoing fermions are not
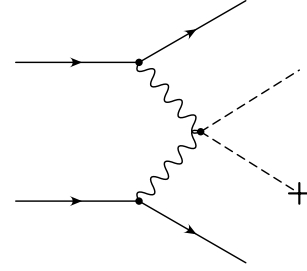

FIG. 1. Higgs production via gauge boson fusion. The solid lines are fermions, wiggly lines are gauge bosons, dashed lines are scalars, and "+" denotes a Higgs VEV.

collinear to the incoming fermions, so that the gauge bosons are off-shell, and Fig. 1 reduces to the effective theory diagram in Fig. 2. The extension to the case where one or both gauge bosons are nearly on-shell is discussed at the end of the paper. There is an important new feature which make the vector boson process particularly interesting — the amplitude is explicitly proportional to the $SU(2) \times U(1)$ symmetry breaking vacuum expectation value (VEV) of the Higgs field v,[1] so that the EFT operator is not a gauge singlet. Gauge invariance of the hard scattering amplitude plays a key role in the development of standard resummation formulæ [1], which can thus no longer be used for this problem. The QCD corrections do not suffer this complication, since they receive no contribution from the Higgs sector.

In the method developed in Refs. [6–10], one first matches onto SCET at a high scale $\mu_h \simeq \sqrt{\hat{s}}$. This matching can be done in the unbroken $SU(3) \times SU(2) \times U(1)$ gauge theory, since symmetry breaking effects are

---

[1] The standard model Lagrangian has a $\phi \to -\phi$ symmetry if the Yukawa couplings are neglected, which would not allow for single Higgs production. This symmetry is broken by the VEV v, and the single Higgs amplitude is proportional to v.
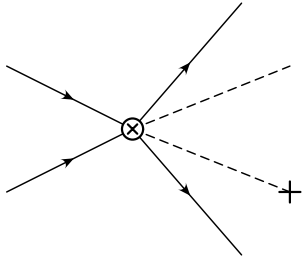
FIG. 2. Higgs production via gauge boson fusion, with the gauge bosons integrated out. Solid lines are fermions, dashed lines are scalars, and "+" denotes a Higgs VEV.

proportional to v, and thus are suppressed by powers of $v/\sqrt{\hat{s}}$. One then runs the effective theory operators to a low scale $\mu_l \simeq M_Z$ using the SCET renormalization group evolution, which sums the $\alpha^n \log^{k \leq 2n} \hat{s}/M_Z^2$ terms. At the low-scale, one integrates out the W and Z, and matches onto a $SU(3) \times U(1)$ effective theory, which only contains gluons and photons. The effects of $SU(2) \times U(1)$ symmetry breaking enter into this low-scale matching. The high-scale matching, and running between the high scale $\mu_h \sim \sqrt{\hat{s}}$ and the low scale $\mu_l \sim M_Z$ can be done using $SU(3) \times SU(2) \times U(1)$ invariant operators in the unbroken theory.

In our scattering process, the incoming and outgoing fermions, and outgoing Higgs particle are energetic, and are treated as collinear fields in SCET. There is also a scalar field ϕ that is replaced by the Higgs VEV $\langle \phi \rangle = v/\sqrt{2}$, and so carries zero four-momentum. The Higgs VEV can be included by matching at the high scale onto gauge-invariant SCET operators with an external soft Higgs field, which is replaced by the Higgs VEV at the low scale μ_l. The SCET operators contain both collinear and soft external fields, and the formalism for including external soft matter fields will be developed in this paper. There is a gauge-invariant soft $\leftrightarrow$ collinear transition operator in the subleading SCET Lagrangian that contributes to the vector boson fusion amplitude, and is derived in Sec. II using tree-level matching. The Lagrangian of Sec. II is used in Sec. III to compute the one-loop form factor for the $\phi^\dagger \phi$ operator. The formalism is then applied to the vector boson fusion amplitude in Sec. IV. The scattering amplitude for energetic external particles (i.e. with collinear external fields) was written in Refs. [9, 10] in terms of process-independent collinear functions, and a soft-function with a universal form. The amplitude for gauge boson fusion can be written in the same way for the fermionic part, with an additional contribution from the Higgs sector. Some subtleties in evaluating SCET integrals using contour integration are discussed in Appendix A. The list of SCET operators for vector boson fusion is given in Appendix B.

Notation: We take all momenta to be incoming, except for the Sudakov case discussed in Sec. III. The light-cone

reference vectors are chosen to be

$$ n_i^\mu = \pm(1, \vec{n}_i), \quad \bar{n}_i^\mu = \pm(1, -\vec{n}_i), \tag{1} $$

where $\vec{n}_i$ points in the direction of particle i. The plus (minus) sign occurs if particle i is incoming (outgoing), except in the Sudakov case where we will always take the plus sign. The group theory generators will be treated as operators $\mathbf{T}_i^a$, which act on particle j as,

$$ \begin{aligned} \left(\mathbf{T}_i^a \psi_j \right)_\alpha &= -T_{\alpha\beta}^a \psi_{j\beta}\, \delta_{ij}, \\ \left(\mathbf{T}_i^a \bar{\psi}_j \right)_\alpha &= \bar{\psi}_{j\beta} T_{\beta\alpha}^a\, \delta_{ij}. \end{aligned} \tag{2} $$

The covariant derivative is $iD = i\partial - gA$. The scalar multiplet is

$$ \phi = \frac{1}{\sqrt{2}} \begin{pmatrix} \varphi^2 + i\varphi^1 \\ v + h - i\varphi^3 \end{pmatrix}, \tag{3} $$

where φ^a are the unphysical Goldstone bosons, and h is the Higgs. The $\lambda \phi^4$ coupling is normalized so that the Higgs mass is $M_h^2 = 2\lambda v^2$, with $v \sim 246$ GeV.

II. THE EFFECTIVE THEORY LAGRANGIAN

In this section, we review the standard form of the SCET operators for processes involving external collinear fields, and then extend the results to operators involving external soft and collinear fields. We will compute the tree-level matching explicitly, and show how the Wilson lines contained in the operators are built up. The subleading SCET Lagrangian contains transition operators between soft and collinear fields, which we derive from this tree-level matching calculation, and will need to study gauge boson fusion.

The effective theory discussed here is SCET_{EW} studied in Refs. [6–10]. The n_i-collinear fields describe particles with momentum p_i near the n_i direction, which scale like $\bar{n}_i \cdot p_i \sim \sqrt{\hat{s}}$, $n_i \cdot p_i \sim \lambda^2 \sqrt{\hat{s}}$ and $p_{i\perp} \sim \lambda \sqrt{s}$. Here $\lambda \sim M/\sqrt{\hat{s}} \ll 1$ is the SCET power counting parameter (not to be confused with the Higgs self-coupling), and M is the gauge boson mass. There is also a mass-mode field, which contains massive gauge bosons with all momentum components scaling like $\lambda\sqrt{\hat{s}} \sim M$. To describe the VEV in the unbroken phase of the gauge theory, we include a soft scalar field with momentum $p_0^\mu \sim \lambda^2 \sqrt{\hat{s}}$.

Consider first a hard-scattering process with r external energetic particles, in directions n_i, $i = 1, \ldots, r$. The effective interaction can schematically be represented as an operator

$$ \prod_i \psi_i, \tag{4} $$

where all the fields are treated as incoming for notational simplicity, and ψ represents fermions or scalars. The gauge indices on the full theory fields ψ_i are combined to form a gauge-invariant operator. At the high scale
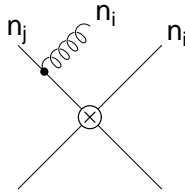
FIG. 3. Collinear gauge boson interactions which generate the collinear Wilson lines.
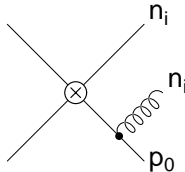

FIG. 4. Collinear gauge boson interactions with a soft field, which generate the collinear Wilson lines and the subleading interaction in Eq. (9).
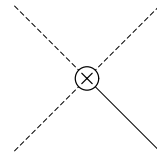

FIG. 5. SCET vertex corresponding to Eq. (7). The dashed lines are collinear fields, and the solid line is a soft field.
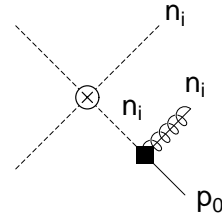

FIG. 6. Graph involving the soft-collinear transition vertex, denoted by a "■". The dashed lines are collinear fields, and the solid line is a soft field.

$\mu_h \sim \sqrt{\hat{s}}$, the operator in Eq. (4) is matched onto an SCET operator with r external collinear fields,

$$\prod_i (W_{n_i}^\dagger \xi_{n_i}) = \prod_i \chi_{n_i}, \qquad \chi_{n_i} \equiv W_{n_i}^\dagger \xi_{n_i}, \qquad (5)$$

where ξ_{n_i} is a collinear field for energetic particles moving in the direction n_i, and W_{n_i} is a n_i-collinear Wilson line. The combination $\chi_{n_i} = W_{n_i}^\dagger \xi_{n_i}$ is gauge invariant under n_i-collinear gauge transformations.

It is instructive to see the origin of the collinear Wilson lines. If n_i-collinear gauge bosons interact with energetic particles moving in the n_j direction (see Fig. 3), the intermediate particles are off shell by an amount of order $\sqrt{\hat{s}}$, and can be integrated out. The resulting operator is a Wilson line involving n_i-collinear gauge bosons, transforming according to the representation $\mathfrak{R}_j$ of particle j. The n_i-collinear Wilson lines for all particles n_j, $j = 1, \ldots, r$ with $j \neq i$ are combined into a n_i-collinear Wilson line transforming as the complex conjugate representation of particle i, $\overline{\mathfrak{R}}_i$. This is because the gauge indices of the operator in Eq. (4) are combined to form a gauge singlet, so the tensor product $\otimes_{j \neq i} \mathfrak{R}_j$ of the Wilson lines combine into a single Wilson line transforming as $\overline{\mathfrak{R}}_i$. This allows the interaction to be written as in Eq. (5), with a single Wilson line $W_{n_i}^\dagger$ for each collinear direction n_i, transforming in the representation $\overline{\mathfrak{R}}_i$ conjugate to particle i.[2]

For the Higgs production amplitude of Fig. 2, we need an interaction of the form Eq. (4), where one of the scalar fields has a momentum which is soft. We will label the soft scalar field by index 0, and the collinear fields by

index i, $i = 1, \ldots, r - 1$. We now perform the matching from the full theory onto SCET analogous to the matching of Eq. (4) onto Eq. (5) in the case where all the particles are collinear. The emission of an n_i-collinear gauge boson from the n_j-collinear particle produces a n_i-collinear Wilson line transforming under the representation $\mathfrak{R}_j$, as before. However, these do not combine into a single Wilson line transforming as $\overline{\mathfrak{R}}_i$, because the soft field is not a gauge singlet.

There are of course also graphs where the n_i collinear gauge boson is emitted from the soft line, as shown in Fig. 4. The one-gauge boson emission graph in Fig. 4 is, for an external soft scalar, proportional to

$$\frac{(2p_0+k)\cdot\varepsilon}{(p_0+k)^2 - m^2} = \frac{\bar{n}_i\cdot\varepsilon}{\bar{n}_i\cdot k} + \left[\frac{(2p_0+k)\cdot\varepsilon}{(p_0+k)^2 - m^2} - \frac{\bar{n}_i\cdot\varepsilon}{\bar{n}_i\cdot k}\right], \quad (6)$$

where p_0 and the gauge boson momentum k are incoming, p_0 is soft and k is n_i collinear, ε is the gauge boson polarization and m is the mass of the scalar multiplet ϕ. The first term generates a n_i-collinear Wilson line transforming as the representation $\mathfrak{R}_0$ of the soft particle. Combined with the n_i-collinear Wilson lines generated by gauge boson emission from the collinear lines n_j ($j \neq i$), this produce a single Wilson line transforming as $\overline{\mathfrak{R}}_i$. This leads to an EFT vertex of the form

$$\psi_0 \prod_{i=1}^{r-1} (W_{n_i}^\dagger \xi_{n_i}) = \psi_0 \prod_{i=1}^{r-1} \chi_{n_i}, \qquad (7)$$

which can be represented graphically as in Fig. 5.

The remaining terms in Eq. (6) reduce to

$$\frac{1}{(p_0 + k)^2 - m^2} \frac{1}{\bar{n}_i\cdot k} \left[(k\cdot\varepsilon)(\bar{n}_i\cdot k) - (\bar{n}_i\cdot\varepsilon)k^2\right], \quad (8)$$

to leading order in the SCET power counting. This additional contribution is given by a new SCET diagram shown in Fig. 6. The new vertex "■", shown in

---

[2] There are important subtleties which arise because of the regulator used in SCET, which are discussed in Refs. [9, 20, 21].
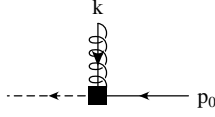
FIG. 7. The soft-collinear transition vertex.

Fig. 7, arises from a gauge-invariant term in the subleading SCET Lagrangian

$$L = -ig \sum \left(\xi_n^\dagger \frac{\bar{n}_\mu \Pi_{n,\nu}}{\bar{n}\cdot\Pi_n} F_n^{\mu\nu} W_n \right) \psi_0 + \text{h.c.}. \qquad (9)$$

Here the collinear covariant derivative Π_n is given by $\Pi_n^\mu = \mathcal{P}_n^\mu - g A_n^\mu$, $\mathcal{P}_n$ is the label momentum operator and A_n^μ and $F_n^{\mu\nu}$ are the n-collinear gauge field and field strength. [Note that $n \cdot \Pi_n$ does not appear in Eq. (9).] Eq. (9) gives the Feynman rule

$$-igT^a \frac{1}{\bar{n}\cdot k} \left[(\bar{n}\cdot k)k^\alpha - k^2 \bar{n}^\alpha \right], \qquad (10)$$

for one-gauge boson emission. The additional factor $1/[(p_0 + k)^2 - m^2]$ needed to get Eq. (8) arises from the intermediate collinear propagator. The operator at the hard vertex "$\otimes$" in Fig. 6 has two collinear fields in the n_i direction, one of which gets turned into a soft field by the new vertex. This soft $\leftrightarrow$ collinear transition vertex does not contribute to the computations in Refs. [9, 10], which only looked at processes with external collinear particles in different directions.

In terms of the SCET B field,

$$B_n^\nu = \frac{i}{\bar{n}\cdot\Pi_n} \bar{n}_\mu F_n^{\mu\nu}, \qquad (11)$$

Eq. (9) is[3]

$$L = -g \sum \left(\xi_n^\dagger \Pi_{n,\nu} B_n^\nu W_n \right) \psi_0 + \text{h.c.}. \qquad (12)$$

The (unspecified) sums in Eqs. (9) and (12) run over all possible values of the label momenta, subject to momentum conservation, and over all possible collinear directions n. The label momenta have to be nonzero on collinear fields to avoid double counting the soft degrees of freedom, so the label sum excludes the zero-bin [21]. This will be important later on.

If the soft particle is a fermion, the corresponding subleading SCET Lagrangian is

$$L = -ig \left(\bar{\xi}_n \frac{\bar{n}_\mu \gamma_\nu^\perp}{\bar{n}\cdot\Pi} F_n^{\mu\nu} W_n \right) \psi_0 + \text{h.c.}$$
$$= -g \left(\bar{\xi}_n \slashed{B}_n^\perp W_n \right) \psi_0 + \text{h.c.}. \qquad (13)$$

---

[3] One may remove the $n\cdot B_n$ dependence in Eq. (12), by using the equations of motion, to write the Lagrangian in terms of standard building blocks, ξ_n, ψ_0 and $B_{n\perp}$ [22]. This removes the single gluon emissions from the subleading Lagrangian and introduces a $\xi_n^\dagger \xi_n \xi_n^\dagger \psi_0$ contact interaction. This field redefinition changes the diagrams in Sec. III, but the result for the total on-shell scattering amplitude is unaffected.

The case of soft fermions has been extensively studied in the literature [23–25]. The interaction Eq. (13) has been obtained previously [26] using reparametrization invariance [27, 28].

More transition operators are generated at higher order in perturbation theory, but will not be required for our analysis as they are higher order in the power counting. For example, at order g^2 for soft scalar particles, there is also the interaction term

$$L = g^2 \sum (\xi_n^\dagger B_{n,\perp\alpha} B_{n,\perp}^\alpha W_n)\psi_0, \qquad (14)$$

which can be obtained by matching the two-gauge boson amplitude onto the effective theory.

We conclude this section with a brief discussion of SCET in the broken phase. An important difference between the broken and unbroken phases is in the choice of gauge-fixing term. While the Lagrangian depends on the gauge-fixing term, the S-matrix does not.

We start by deriving SCET in the broken phase from the full theory in the broken phase. In the unbroken theory we used Feynman gauge with gauge fixing term

$$-\frac{1}{2} \left(\partial^\mu A_\mu^a \right)^2, \qquad (15)$$

whereas in the broken theory we will use $R_{\xi=1}$ gauge with gauge fixing term

$$-\frac{1}{2} \left(\partial^\mu A_\mu^a + M\varphi^a \right)^2. \qquad (16)$$

Here φ^a are the Goldstone bosons in Eq. (3) and M is the gauge boson mass. The $A\varphi$ cross-terms from the R_ξ gauge-fixing term cancel the $A\varphi$ mixing terms in the kinetic energy of the scalar, and the Goldstone bosons obtain a mass M. In Feynman gauge, the gauge boson can couple the VEV to an intermediate φ particle, but such a coupling is absent in the R_ξ gauge. Thus, there are no emissions from the line associated with the VEV in R_ξ gauge. In particular, we do not get the contribution in the $\mathfrak{R}_0$ representation to the n_i-collinear Wilson line, which was present in the unbroken phase.

Alternatively, we may obtain SCET in the broken phase from SCET in the unbroken phase by changing the gauge-fixing term, which should lead to the same result. For simplicity, we only show that the contributions to the emission of a single gauge boson from the line associated with the VEV cancel. Adding up the contribution from the Wilson line W_n, the contribution from the subleading Lagrangian in Eq. (9), where ψ_0 has been replaced by its VEV, and the contribution from the gauge-fixing term in Eq. (16), we get

$$\frac{\bar{n}^\alpha}{\bar{n}\cdot k} + \frac{1}{k^2 - M^2}\frac{1}{\bar{n}\cdot k}\left[(\bar{n}\cdot k)k^\alpha - k^2\bar{n}^\alpha\right] - \frac{1}{k^2 - M^2}k^\alpha$$
$$= -\frac{1}{k^2 - M^2}\frac{1}{\bar{n}\cdot k}M^2\bar{n}^\alpha, \qquad (17)$$

where we have left out an overall factor of $M = gv/2$. The terms do not seem to cancel. However, there is another contribution due to a subtlety when switching to
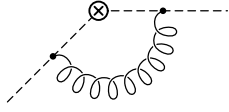
FIG. 8. One-loop scattering of a scalar field by the external operator $\phi^\dagger\phi$.
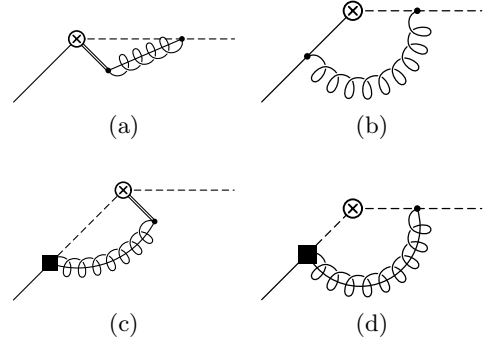

FIG. 9. One-loop EFT diagrams of the scattering of a scalar field by the external operator $\phi^\dagger\phi$. Graph (a) is the n-collinear graph D_n, (b) is the soft graph $\widetilde{D}_s$, and (c) and (d) are graphs D_1 and D_2 involving the soft-collinear transition vertex. Dashed lines are collinear scalars, and solid lines are soft scalars. The double line denotes a Wilson line.

the broken phase. In the unbroken phase, the soft field is of order $\psi_0 \sim \lambda^2$, where λ is the power counting parameter (not to be confused with the Higgs self-coupling). In the broken phase we get $\langle\psi_0\rangle \sim M \sim \lambda$, so its power counting changes. This implies that subleading terms in the unbroken Lagrangian can get promoted to leading order, when switching to the broken phase. Using $\phi \to \xi_n + W_n\psi_0$, decomposing ϕ and ξ_n as in Eq. (3), we obtain

$$-\frac{1}{2}M^2\varphi^a\varphi^a = -\frac{1}{2}M^2\left(\varphi_n^a\varphi_n^a + iv\frac{g\bar{n}\cdot A_n}{\bar{n}\cdot k}\varphi_n^a + \dots\right),\text{(18)}$$

from the Goldstone boson mass term by emitting a gauge boson from the Wilson line. The second term on the right hand side is a subleading term that gets promoted to leading order when ϕ_0 gets a VEV. It gives the missing contribution necessary to cancel Eq. (17).

III. ONE LOOP

A nontrivial check of the results of the previous section is to verify that the effective theory correctly reproduces the infrared structure of the full theory at the one-loop level. The process we will consider is shown in Fig. 8: the one-loop scattering of a scalar field by the external operator $\phi^\dagger\phi$. The incoming scalar momentum p_0 is taken to be soft, the outgoing scalar momentum p_f is taken to be collinear and we will assume for simplicity that the external particles are massless. The general scattering process of this kind, such as vector boson fusion in Fig. 2, has several collinear particles and one soft particle. There, the one-loop vertex graphs are a sum of graphs connecting two collinear particles, or a collinear particle with a soft particle. We already know that the infrared behavior of the collinear-collinear graphs in the full and effective theories agree. If the effective theory correctly reproduces Fig. 8, then it will also correctly reproduce the collinear-soft graphs, and hence the total one-loop correction. We will apply the results derived here to vector boson fusion in Sec. IV.

The vertex graph depends on $p_0 \cdot p_f$ and the gauge boson mass M^2. Since p_f is collinear and p_0 is soft, $p_0\cdot p_f \sim \lambda^2\hat{s}$, where λ is the SCET power counting parameter. The SCET power counting for the massive gauge theory is such that $\lambda^2 \sim M^2/\hat{s}$, so that $p_0 \cdot p_f \sim M^2$. This scale is not a hard scale and does not get integrated out, so the effective theory must reproduce the entire $p_0 \cdot p_f/M^2$ dependence of the vertex graph. Eventually, we are interested in the case $p_0 \to 0$, since the soft field

will turn into the Higgs VEV. The on-shell vertex graph in the full theory is

$$D_F = \frac{\alpha}{4\pi}\mathbf{T}_0\cdot\mathbf{T}_f\, I_F\,,$$

$$I_F = i(4\pi)^2 f_\epsilon \int \frac{\mathrm{d}^d k}{(2\pi)^d}\frac{(2p_0+k)\cdot(2p_f+k)}{(k+p_0)^2(k+p_f)^2(k^2-M^2)}$$

$$= -\frac{1}{\epsilon} - \log\frac{Q^2}{\mu^2} + 2\log\frac{M^2}{\mu^2}$$

$$+ \left(2-\frac{M^2}{Q^2}\right)\left[\frac{\pi^2}{6} - \mathrm{Li}_2\left(1-\frac{Q^2-i0^+}{M^2}\right)\right],\text{(19)}$$

with $Q^2 = -(p_0-p_f)^2$ and $f_\epsilon = (4\pi)^{-\epsilon}\mu^{2\epsilon}e^{\epsilon\gamma_E}$. In anticipation of the more general case needed for vector boson fusion, we have factored the gauge group generators from the integral I_F. For the form-factor calculation with only two particles, $\mathbf{T}_f + \mathbf{T}_0 = 0$ since the vertex is a gauge singlet, so that $-\mathbf{T}_f \cdot \mathbf{T}_0 = \mathbf{T}_f^2 = \mathbf{T}_0^2 = C_F$.

Including the wave-function graphs gives the scalar form factor

$$F_S = \frac{\alpha C_F}{4\pi}\left\{\frac{3}{\epsilon} + \log\frac{Q^2}{\mu^2} - 4\log\frac{M^2}{\mu^2} + \frac{3}{2}\right.$$

$$\left. - \left(2-\frac{M^2}{Q^2}\right)\left[\frac{\pi^2}{6} - \mathrm{Li}_2\left(1-\frac{Q^2-i0^+}{M^2}\right)\right]\right\},\text{(20)}$$

which is gauge invariant. If $Q^2 = 0$, as is the case for a VEV ($p_0 = 0$),

$$I_F = -\frac{1}{\epsilon} + \log\frac{M^2}{\mu^2} - 1\,,$$

$$F_S = \frac{\alpha C_F}{4\pi}\left(\frac{3}{\epsilon} - 3\log\frac{M^2}{\mu^2} + \frac{5}{2}\right).\text{(21)}$$

We will now calculate the graphs in the EFT, regulating the IR using the Δ regulator [20]. This introduces the regulator parameters Δ_f and δ_f for the collinear field,

which are related by

$$\delta_f \equiv \frac{\Delta_f}{\bar{n}\cdot p_f}\,. \tag{22}$$

It is not necessary to introduce an IR regulator for the soft particle for computing the zero-bin subtracted diagrams.

The graph Fig. 9(a) is the usual n-collinear graph where the gauge boson couples to the outgoing field, and to the n-collinear Wilson line W_n at the hard vertex. The diagram yields the integral

$$D_n = \frac{\alpha}{4\pi}\mathbf{T}_f^2\,I_n\,, \tag{23}$$

$$I_n = -i(4\pi)^2 f_\epsilon \int \frac{\mathrm{d}^d k}{(2\pi)^d}\frac{1}{k^2 - M^2}\frac{\bar{n}\cdot(2p_f + k)}{\bar{n}\cdot k\,[(k+p_f)^2 - \Delta_f]}\,,$$

and the zero-bin subtraction is

$$I_{n,\o} = -i(4\pi)^2 f_\epsilon \int \frac{\mathrm{d}^d k}{(2\pi)^d}\frac{1}{k^2 - M^2}$$
$$\times \frac{2\bar{n}\cdot p_f}{\bar{n}\cdot k\,[(\bar{n}\cdot p_f)(n\cdot k) - \Delta_f]}, \tag{24}$$

which combine to give [20]

$$I_n - I_{n,\o} = \frac{2}{\epsilon^2} - \frac{2}{\epsilon}\log\frac{\Delta_f}{\mu^2} + \frac{1}{\epsilon} - \log^2\frac{M^2}{\mu^2}$$
$$- \left(1 - 2\log\frac{\Delta_f}{\mu^2}\right)\log\frac{M^2}{\mu^2} - \frac{\pi^2}{2} + 1. \tag{25}$$

The zero-bin subtracted collinear graph depends only on the properties of p_f, and is independent of the properties of the other particle p_0. This is an example of factorization, for which zero-bin subtractions are crucial.

Fig. 9(b) is due to soft gauge boson exchange between the soft and collinear lines,

$$\widetilde{D}_s = \frac{\alpha}{4\pi}\mathbf{T}_0\cdot\mathbf{T}_f\,\widetilde{I}_s\,, \tag{26}$$

$$\widetilde{I}_s = i(4\pi)^2 f_\epsilon \int\frac{\mathrm{d}^d k}{(2\pi)^d}\frac{1}{k^2 - M^2}\frac{1}{n\cdot k - \delta_f}\frac{n\cdot(2p_0 + k)}{(k+p_0)^2}\,.$$

The "$\sim$" is a reminder that this soft diagram is different from I_s in deep inelastic scattering [29], where the soft gauge boson exchange is between two collinear lines. We evaluate $\widetilde{I}_s$ by performing the k^+ integral by contours, followed by the $k_\perp$ and k^- integrals, yielding[4]

$$\widetilde{I}_s = -\frac{1}{\epsilon} + \log\frac{M^2}{\mu^2} - 1 - (2+\tau)G(\tau)\,, \tag{27}$$

where

$$G(\tau) = \left(\frac{1}{\epsilon} - \log\frac{M^2}{\mu^2}\right)\log\frac{\tau}{1+\tau} - \mathrm{Li}_2\left(\frac{1}{1+\tau}\right), \tag{28}$$

---

[4] Some tricky aspects of evaluating SCET integrals using contours are discussed in Appendix A. Alternatively, one can combine the linear and quadratic propagators using the modified Feynman parameter method as in HQET.

and

$$\tau = \frac{\Delta_f}{Q^2}\,. \tag{29}$$

The Δ_f is a regulator, so the integrals are evaluated with $\Delta_f \to 0$. However, we want to study the vertex correction where p_0 is soft, but nonzero, and also the case where p_0 is exactly 0. Depending on whether $Q^2 = 0$ or $Q^2 \neq 0$, the $\Delta_f \to 0$ limit corresponds to $\tau \to \infty$ or $\tau \to 0$. We therefore retain the entire τ dependence, and show that it cancels in the final result. If $Q^2 = 0$ so that $\tau = \infty$, $\widetilde{I}_s = 0$.

There are also several diagrams involving the soft-collinear transition vertex. Fig. 9(c) arises from the gauge boson in the transition vertex coupling to the Wilson line W_n at the hard-scattering vertex,

$$D_1 = \frac{\alpha}{4\pi}\mathbf{T}_0\cdot(\mathbf{T}_0 + \mathbf{T}_f)\,I_1\,, $$

$$I_1 = -i(4\pi)^2 f_\epsilon \int\frac{\mathrm{d}^d k}{(2\pi)^d}\frac{1}{k^2 - M^2}\frac{1}{(k+p_0)^2}$$
$$= \frac{1}{\epsilon} - \log\frac{M^2}{\mu^2} + 1\,. \tag{30}$$

The gauge group factor for this graph is different from the other diagrams. The hard vertex is the operator $\bar{\chi}_{n_f}\chi_{n_f} = (\xi_{n_f}^\dagger W_{n_f})(W_{n_f}^\dagger\xi_{n_f}) = \xi_{n_f}^\dagger\xi_{n_f}$, where the Wilson lines cancel since the fields fields have the same collinear direction. Graph Fig. 9(c) is therefore absent in the form-factor calculation. We also want to apply the results of this section to the case where there are many collinear particles at the vertex. In this case, the gauge group factor for Fig. 9(c) is $\mathbf{T}_0\cdot(\mathbf{T}_0 + \mathbf{T}_f)$ rather than $\mathbf{T}_0\cdot\mathbf{T}_f$ as for the other graphs in the figure. However, the zero-bin subtraction for graph D_1 is

$$I_{1,\o} = I_1\,, \tag{31}$$

so that the zero-bin subtracted diagram $I_1 - I_{1,\o}$ vanishes. Thus Fig. 9(c) does not contribute even in the more general case of processes with several external particles.

Fig. 9(d) arises from the gauge boson in the transition vertex coupling directly to the outgoing collinear field and is given by

$$D_2 = \frac{\alpha}{4\pi}\mathbf{T}_0\cdot\mathbf{T}_f\,I_2\,, $$

$$I_2 = i(4\pi)^2 f_\epsilon \int\frac{\mathrm{d}^d k}{(2\pi)^d}\frac{1}{k^2 - M^2}\frac{1}{(k+p_0)^2}$$
$$\times\frac{\bar{n}\cdot k\,(2p_f + k)\cdot k - k^2\,\bar{n}\cdot(2p_f + k)}{\bar{n}\cdot k\,[(k+p_f)^2 - \Delta_f]}\,. \tag{32}$$

The corresponding zero-bin subtraction is

$$I_{2,\o} = i(4\pi)^2 f_\epsilon \int\frac{\mathrm{d}^d k}{(2\pi)^d}\frac{1}{k^2 - M^2}\frac{1}{(k+p_0)^2}$$
$$\times\frac{\bar{n}\cdot k\,n\cdot k - 2k^2}{\bar{n}\cdot k\,(n\cdot k - \delta_f)}\,. \tag{33}$$
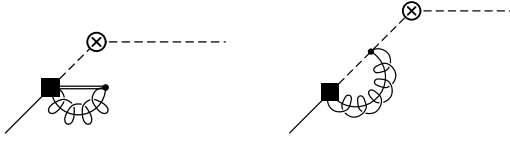
FIG. 10. Additional graphs involving the soft-collinear transition vertex, whose contribution vanishes. The dashed lines are collinear fields, and the solid line is a soft field.
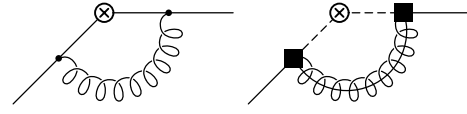

FIG. 11. Vertex graphs when both external particles are soft. The first graph has a soft gauge boson, and the second has a collinear gauge boson. The dashed lines are collinear fields, and the solid lines are soft fields.

It is convenient to write

$$I_2 = I_n + \overline{I}_2, \qquad I_{2,\text{ø}} = I_{n,\text{ø}} + \overline{I}_{2,\text{ø}}, \qquad (34)$$

where I_n is the n-collinear integral of Eq. (23), and similarly for the zero-bin subtraction. This gives easier integrals to evaluate,

$$\overline{I}_2 = -\frac{1}{\epsilon} - \log\frac{Q^2}{\mu^2} + 2\log\frac{M^2}{\mu^2}$$
$$+ \left(2 - \frac{M^2}{Q^2}\right)\left[\frac{\pi^2}{6} - \text{Li}_2\left(1 - \frac{Q^2}{M^2}\right)\right],$$
$$\overline{I}_{2,\text{ø}} = -\frac{1}{\epsilon} + \log\frac{M^2}{\mu^2} - 1 - (2+\tau)G(\tau). \qquad (35)$$

On comparing with Eq. (19) and Eq. (27), we find that $\overline{I}_2 = I_F$, $\overline{I}_{2,\text{ø}} = \widetilde{I}_s$.

There are additional graphs involving the soft-collinear transition vertex, given in Fig. 10. The first graph arises from the gauge boson in the transition vertex coupling to W_n in the transition vertex, and the second from the gauge boson coupling directly to the incoming collinear line. These graphs turn the incoming p_0 line into a collinear line, which cannot conserve label momentum since the sums in Eqs. (9) and (12) exclude the zero-bin. Their contribution therefore vanishes.

The total vertex correction in the effective theory is the sum of the zero-bin subtracted graphs in Fig. 8,

$$\frac{\alpha}{4\pi}[\mathbf{T}_f^2(I_n - I_{n,\text{ø}}) + \mathbf{T}_0\cdot\mathbf{T}_f(\widetilde{I}_s + I_2 - I_{2,\text{ø}})]$$
$$= \frac{\alpha}{4\pi}[\mathbf{T}_f\cdot(\mathbf{T}_0 + \mathbf{T}_f)(I_n - I_{n,\text{ø}}) + \mathbf{T}_0\cdot\mathbf{T}_f\, I_F]. \quad (36)$$

For the form factor, gauge invariance $\mathbf{T}_0 + \mathbf{T}_f = 0$ implies that this is equal to the full theory vertex graph D_F. The wave-function graphs for the two particles in the full and effective theories also agree, so that the on-shell form factors are equal in the two theories. The entire regulator dependence of the EFT graphs cancels, and zero-bin subtractions [21] in the EFT theory are necessary for the EFT to correctly reproduce the full theory.

The above computation also shows that the one-loop contribution to the matching for the soft-collinear form factor vanishes since the full and effective theory results agree. This is in contrast to e.g. deep inelastic scattering, where the incoming and external particles are collinear fermions scattered by the electromagnetic current. There the full and effective theory results differ by

a finite matching correction [29]

$$C(Q^2,\mu) = \frac{\alpha(\mu)C_F}{4\pi}\left(-\log^2\frac{Q^2}{\mu^2} + 3\log\frac{Q^2}{\mu^2} + \frac{\pi^2}{6} - 8\right),$$
$$(37)$$

which only depends on the short-distance scale Q^2, and is independent of any infrared physics. In our computation, Q^2 is no longer a hard scale, so the entire Q^2 dependence must be reproduced by the effective theory.

We have explicitly shown the agreement between the full and effective theories for the scalar-scalar form factor with vertex $\phi^\dagger\phi$. One can similarly check agreement for other form factors, such as the scalar-fermion form factor with vertex $\bar{\psi}\phi$, etc. The computations are very similar to the scalar-scalar case, and will not be given here.

Lastly, the form factor when both external particles are soft is given by the graphs in Fig. 11. The first diagram, with a soft gauge boson loop, reproduces the full theory graph. The soft-collinear transition vertex Eq. (9) gives the second graph shown in the figure. The internal particles are n-collinear, but the external particles are soft. There is nothing in the kinematics to fix the collinear direction n, and the graph does not depend on any external collinear momenta. After zero-bin subtraction, the graph vanishes for any n, as it should.

IV. VECTOR BOSON FUSION

The previous section treated the one-loop form factor for scalar production by $\phi^\dagger\phi$. We can now apply the formalism to vector boson fusion. We will compute the EFT amplitude, which consists of the running between μ_h and μ_l, and the low-scale matching. This sums all the large logarithms in the scattering amplitude. The remaining details, such as the high-scale matching and numerical results, will be given in Ref. [30].

The Higgs part of the vector boson fusion process is described by the operators $\phi^\dagger\phi$ and $\phi^\dagger T^a\phi$, which come from WW, WB and BB in the kinetic term for ϕ. At the high scale, these operators match onto two terms in SCET,

$$\phi^\dagger\phi \to \left(\phi_n^\dagger W_n\right)\phi_0 + \phi_0^\dagger\left(W_n^\dagger\phi_n\right),$$
$$\phi^\dagger T^a\phi \to \left(\phi_n^\dagger W_n\right)T^a\phi_0 + \phi_0^\dagger T^a\left(W_n^\dagger\phi_n\right). \quad (38)$$

The first term on each line has $\phi^\dagger$ replaced by a collinear scalar field $\phi_n^\dagger$, and the ϕ field replaced by a soft field ϕ_0.

In the second term, the roles of ϕ and $\phi^\dagger$ are reversed. The collinear fields $(\phi_n^\dagger W_n)$ and $(W_n^\dagger \phi_n)$ both have momentum equal to p_h, the momentum of the Higgs particle. In this section we take all momenta to be incoming, in contrast to the previous section. The SCET operators that we will need for vector boson fusion are

$$
\begin{aligned}
\mathcal{O}_1 &= \left[\left(\phi_n^\dagger W_n\right) \phi_0 + \phi_0^\dagger \left(W_n^\dagger \phi_n\right) \right] O\,, \\
\mathcal{O}_2 &= \left[\left(\phi_n^\dagger W_n\right) T^a \phi_0 - \phi_0^\dagger T^a \left(W_n^\dagger \phi_n\right) \right] O^a\,, \\
\mathcal{O}_3 &= \left[\left(\phi_n^\dagger W_n\right) \phi_0 - \phi_0^\dagger \left(W_n^\dagger \phi_n\right) \right] O\,, \\
\mathcal{O}_4 &= \left[\left(\phi_n^\dagger W_n\right) T^a \phi_0 + \phi_0^\dagger T^a \left(W_n^\dagger \phi_n\right) \right] O^a\,, \quad (39)
\end{aligned}
$$

where O contains the remaining fermions, which are collinear fields in different directions. (A complete basis for O and O^a is given in Appendix B.) As is clear from Eq. (38), the operators $\mathcal{O}_2$ and $\mathcal{O}_3$ do not get matched on to at the high scale. However, the running generates these operators and they contribute to the low-scale matching.

At tree level, the low-scale matching amounts to picking out the h component of ϕ_n or $\phi_n^\dagger$, and the v component of ϕ_0 or $\phi_0^\dagger$,

$$
\begin{aligned}
(\phi_n^\dagger W_n)\phi_0 &\to \frac{v}{2} h_n\,, & \phi_0^\dagger (W_n^\dagger \phi_n) &\to \frac{v}{2} h_n\,, \quad (40) \\
(\phi_n^\dagger W_n) T^a \phi_0 &\to -\frac{v}{4} h_n \delta_{a3}\,, & \phi_0^\dagger T^a (W_n^\dagger \phi_n) &\to -\frac{v}{4} h_n \delta_{a3}\,,
\end{aligned}
$$

where h_n creates collinear Higgs particles (h is a real field). Consequently, $\mathcal{O}_2$ and $\mathcal{O}_3$ do not contribute to the low-scale matching at tree level.

The one-loop amplitude can now be computed using the results of the previous section and the analysis in Ref. [9]. We first calculate the anomalous dimension using the unbroken $SU(2) \times U(1)$. Since the spontaneous symmetry breaking is a low energy effect, it does not affect the renormalization. We then repeat the calculation of the anomalous dimension in the broken phase, and determine the low-scale matching. We conclude this section with a brief discussion of the case where one (or both) of the gauge bosons gets produced on shell.

A. Unbroken Phase

We start this section by considering a general gauge group, and derive the anomalous dimension for an operator with collinear fields $i = 1, r-1$ in distinct collinear directions and a soft scalar field labeled 0. We then specialize to vector boson fusion in the Standard Model and add the contributions from other (non-gauge) interactions.

Adding up the one-loop gauge boson exchange diagrams, we obtain

$$
\begin{aligned}
\frac{\alpha}{4\pi} \Big[&\sum_i \mathbf{T}_i^2 \big(I_n^i - I_{n,\varnothing}^i\big) + \sum_{(ij)} \mathbf{T}_i \cdot \mathbf{T}_j I_s^{ij} \quad (41) \\
&+ \sum_i \mathbf{T}_i \cdot \mathbf{T}_0 \big(I_n^i - I_{n,\varnothing}^i + I_F^i\big) \Big] + \sum_i \frac{1}{2}\delta R^i + \frac{1}{2}\delta R^\phi\,.
\end{aligned}
$$

Here the sum on i runs over the collinear fields, but not the soft field. The first term corresponds to the collinear graph in Fig. 9(a) given by $I_n - I_{n,\varnothing}$. We included the superscript "i" everywhere to account for the different particle types (scalar or fermion). The sum on (ij) in the second term runs over pairs of collinear fields, and describes the contribution I_s from soft gauge boson exchange between the two collinear fields (not to be confused with $\widetilde{I}_s$). We take the momentum of the soft scalar field p_0 to be exactly zero, so the only remaining diagram is Fig. 9(d), which we write as $I_2 = I_n - I_{n,\varnothing} + I_F$. The final terms are the wave-function contribution δR^i for the collinear fields and δR^ϕ for the soft scalar field. Using gauge invariance of the operator, $\mathbf{T}_0 + \sum_i \mathbf{T}_i = 0$, we see that the Δ regulators cancel.

From the divergent terms in Eq. (41), we obtain the one-loop anomalous dimension

$$
\begin{aligned}
\gamma_\mathcal{O} = \frac{\alpha}{4\pi} \Big\{ &\sum_{i \in \phi} \Big[\mathbf{T}_i^2 \Big(4\log\frac{\bar{n}_i \cdot p_i}{\mu} - 4\Big) + \mathbf{T}_i \cdot \mathbf{T}_0 \Big(4\log\frac{\bar{n}_i \cdot p_i}{\mu}\Big) \Big] \\
&+ \sum_{i \in \psi} \Big[\mathbf{T}_i^2 \Big(4\log\frac{\bar{n}_i \cdot p_i}{\mu} - 3\Big) + \mathbf{T}_i \cdot \mathbf{T}_0 \Big(4\log\frac{\bar{n}_i \cdot p_i}{\mu} - 2\Big) \Big] \\
&- 4\sum_{(ij)} \mathbf{T}_i \cdot \mathbf{T}_j \log\frac{-n_i \cdot n_j - i0}{2} - 2\mathbf{T}_0^2 \Big\}\,. \quad (42)
\end{aligned}
$$

Here we separated the sum into a sum over collinear scalars ($i \in \phi$) and collinear fermions ($i \in \psi$). We immediately identify the usual collinear and soft functions [9, 10], but there are additional terms involving $\mathbf{T}_i \cdot \mathbf{T}_0$ or $\mathbf{T}_0^2$, which need to be included. Define $\tilde{\gamma}_\mathcal{O}$ to be the anomalous dimension for the SCET vector boson fusion operator, given by summing over the soft and collinear functions for all the external particles (i.e. fermions and Higgs, but not the VEV). Then the total anomalous dimension is

$$
\begin{aligned}
\gamma_\mathcal{O} = \tilde{\gamma}_\mathcal{O} + \frac{\alpha}{4\pi} \Big[&\mathbf{T}_h \cdot \mathbf{T}_0 \Big(4\log\frac{\bar{n}_h \cdot p_h}{\mu}\Big) - 2\mathbf{T}_0^2 \\
&+ \sum_{i \in \psi} \mathbf{T}_i \cdot \mathbf{T}_0 \Big(4\log\frac{\bar{n}_i \cdot p_i}{\mu} - 2\Big) \Big]\,. \quad (43)
\end{aligned}
$$

For vector boson fusion in the Standard Model, the Higgs wave-function renormalization receives other contributions, such as from the top Yukawa coupling y_t. This is automatically included by using the form in Eq. (43) for the anomalous dimension, since the Higgs collinear function defined in Refs. [9, 10] includes the full Higgs wave-function renormalization. An additional contribution arises from the ϕ rescattering graph in Fig. 12. For
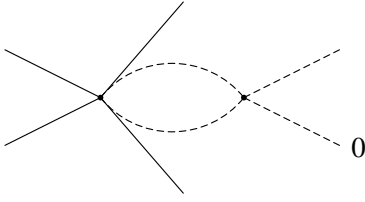
FIG. 12. Radiative correction due to the $\lambda\phi^4$ Higgs self-coupling. The soft field is denoted by 0. The dashed lines are scalars and the solid lines are fermions.

$\mathcal{O}_2$ and $\mathcal{O}_3$ this vanishes due to the relative minus sign between the terms. The integral is the same for $\mathcal{O}_1$ and $\mathcal{O}_4$, but the coefficient differs: from the contractions of $\phi^\dagger\phi$ and $\phi^\dagger T^a\phi$ with $(\phi^\dagger\phi)^2$, we find a relative factor of 3. This leads to an additional contribution to the anomalous dimension

$$\delta\gamma_{\mathcal{O}} = \frac{c^{\mathcal{O}}\lambda}{4\pi^2}\mathbb{1}\,. \qquad (44)$$

where the coefficient $c^{\mathcal{O}} = \{3, 0, 0, 1\}$ for the operator $\{\mathcal{O}_1, \mathcal{O}_2, \mathcal{O}_3, \mathcal{O}_4\}$.

In Refs. [9, 10], there was no λ contribution to the anomalous dimension for Higgs pair production. This is because Higgs pair production has two energetic Higgs fields moving in different directions, described by collinear SCET fields with different labels. The rescattering of two collinear particles moving in different directions by a $\lambda\phi^4$ coupling is power suppressed. In vector boson fusion, one of the scalars is a soft scalar, and soft-collinear scattering is leading order.

In Appendix B a complete basis of SCET operators for vector boson fusion is given, including the action of the $SU(2)$ generators $\mathbf{T}_i \cdot \mathbf{T}_0$ in this basis.

B. Broken Phase

We will now match onto the broken $SU(2) \times U(1)$ to compute the low-scale matching, and verify that the anomalous dimension computed in the broken and unbroken theories are identical. The diagrams are different in the two phases, because of a change in the gauge-fixing term.

At tree level, the $\phi^\dagger\phi$ and $\phi^\dagger T^a\phi$ part of Eq. (39) turn into

$$\mathcal{O}_1 \to \left[(v + h_0)h_n + \varphi_0^a\varphi_n^a\right]O\,,$$
$$\mathcal{O}_2 \to \frac{i}{2}\left[-(v + h_0)\varphi_n^a + \varphi_0^a h_n + \epsilon^{abc}\varphi_0^b\varphi_n^c\right]O^a\,, \quad (45)$$

where φ^a are the unphysical Goldstone bosons. The corresponding expressions for $\mathcal{O}_3$ and $\mathcal{O}_4$ can be obtained from those for $\mathcal{O}_1$ and $\mathcal{O}_2$, by replacing

$$h_n \leftrightarrow i\varphi_n^3\,, \quad \varphi_n^1 \leftrightarrow i\varphi_n^2\,. \qquad (46)$$

The terms in Eq. (45) with more than a single h_n or φ_n^a can contribute to vector boson fusion through e.g. the
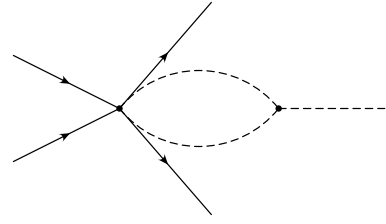
FIG. 13. Radiative correction to Higgs production due to the $\lambda\phi^4$ coupling in the broken phase. The tri-scalar coupling is proportional to λv. The dashed lines are scalars and the solid lines are fermions, which are all collinear.
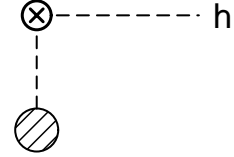

FIG. 14. Tadpole correction to Higgs production. The tadpole amplitude Γ^h is denoted by the shaded blob.

rescattering graph in Fig. 13, which is the analog of Fig. 12 in the broken phase. From the calculation in the unbroken phase, we know that all the terms in Eq. (45) for the same operator have the same renormalization and thus stay together. We can therefore restrict ourselves to graphs with one external collinear scalar to crosscheck the anomalous dimension. Only the graphs with one external Higgs boson contribute to the low-scale matching. In the low-scale matching we get a dependence on the masses of particles for the first time, and also need to take into account that only W and Z (but not γ) get integrated out. The following identity will be useful:

$$\alpha_2\mathbf{T}_i \cdot \mathbf{T}_j + \alpha_1\mathbf{Y}_i\mathbf{Y}_j \qquad (47)$$
$$= \alpha_W(\mathbf{T}_i^+\mathbf{T}_j^- + \mathbf{T}_i^-\mathbf{T}_j^+) + \alpha_Z\mathbf{T}_i^Z\mathbf{T}_j^Z + \alpha_{\rm em}\mathbf{Q}_i\mathbf{Q}_j$$
$$= \alpha_2(\mathbf{T}_i \cdot \mathbf{T}_j - \mathbf{T}_i^3\mathbf{T}_j^3) + (\alpha_2 + \alpha_1)\mathbf{T}_i^Z\mathbf{T}_j^Z + \alpha_{\rm em}\mathbf{Q}_i\mathbf{Q}_j\,,$$

where $\mathbf{T}^\pm = (\mathbf{T}^1 \pm i\mathbf{T}^2)/\sqrt{2}$, $\mathbf{T}^Z = \mathbf{T}^3 - \sin^2\theta_W\mathbf{Q}$, $\mathbf{Y}$ is the hypercharge and $\mathbf{Q}$ is the charge operator.

We will restrict ourselves to studying contributions that involve the Higgs sector. The diagrams are: soft gauge boson exchange between a scalar and a fermion akin to Fig. 8, the collinear graph for a scalar in Fig. 9(a), the scalar wave-function diagram, the rescattering graph in Fig. 13, and the tadpole graph in Fig. 14. In the above we wrote "scalar" to allow for both an external Higgs or Goldstone boson. In the low-scale matching we only need the Higgs contribution.

The soft gauge boson exchange can be written in the same form as in the unbroken phase in Eq. (41), with the understanding that

$$\mathbf{T}_h^a h_n = -\frac{i}{2}\varphi_n^a\,, \quad \mathbf{T}_h^a\varphi_n^b = \frac{i}{2}(\delta^{ab}h_n + \epsilon^{abc}\varphi_n^c)\,, \quad (48)$$

subject to the replacements in Eq. (46) for $\mathcal{O}_3$ and $\mathcal{O}_4$.

These expressions can be obtained using the correspondence with the unbroken phase, e.g.

$$\mathbf{T}_h^a h_n \to \frac{1}{v}\mathbf{T}_h^a\big(\phi_n^\dagger\phi_0 + \phi_0^\dagger\phi_n\big)$$
$$= \frac{1}{v}\big(\phi_n^\dagger T^a\phi_0 + \phi_0^\dagger T^a\phi_n\big) \to -\frac{i}{2}\varphi_n^a. \quad (49)$$

We also need to take the mass of the Goldstone boson $M_\varphi \neq M_h$ into account in the loop integral I_s. This leads to the replacement $\Delta \to \Delta + M_{\rm in}^2 - M_{\rm ex}^2$ for the Δ regulator of the scalar field, where $M_{\rm in}$ is the mass of the scalar in the loop and $M_{\rm ex}$ is the mass of the external scalar. Since the Δ regulators will cancel out, this shift is irrelevant.

In the collinear graph, a gauge boson is emitted from the Wilson line and reabsorbed later. We would therefore need to include the Wilson line contribution in Eq. (45). This diagram can again be described by the same expression as in the broken phase, using Eq. (48) and replacing $\Delta \to \Delta + M_{\rm in}^2 - M_{\rm ex}^2$ in the Δ regulator of the scalar particle. In the low-scale matching, where the external particle is the Higgs, the massive collinear function has an additional term compared to the massless case in Eq. (25)

$$I_n^h - I_{n,\varnothing}^h = \big(I_n - I_{n,\varnothing} \text{ with } \Delta_h \to \Delta_h + M_\varphi^2 - M_h^2\big)$$
$$+ f_S\Big(\frac{M_h^2}{M^2}, \frac{\Delta_h + M_\varphi^2}{M^2}\Big) \quad (50)$$

The function f_S was defined in Appendix B of Ref. [8]

$$f_S(w,z) = \int_0^1 \mathrm{d}x \, \frac{2-x}{x} \log\frac{1-x+zx-wx(1-x)}{1-x}. \quad (51)$$

Since we can set $\Delta_h = 0$ and $M_\varphi = M$, we need

$$f_S(w,1) = 1 + \frac{\pi^2}{3} - 2\sqrt{\frac{w-4}{w}}\tanh^{-1}\sqrt{\frac{w}{w-4}} \quad (52)$$
$$-2\mathrm{Li}_2\frac{w+\sqrt{(w-4)w}}{2} - 2\mathrm{Li}_2\frac{w-\sqrt{(w-4)w}}{2}.$$

As was discussed at the end of section Sec. II, we do not get the $\mathfrak{R}_0$ contribution to the Wilson line in the broken phase. This leads to the replacement $\mathbf{T}_i^2 \to \mathbf{T}_i\cdot(\mathbf{T}_i+\mathbf{T}_0)$ in Eq. (41) for the contribution from the collinear graph. Here $\mathbf{T}_0$ acts like

$$\mathbf{T}_0^a h_n = \frac{i}{2}\varphi_n^a, \quad \mathbf{T}_0^a\varphi_n^b = \frac{i}{2}(-\delta^{ab}h_n + \epsilon^{abc}\varphi_n^c), \quad (53)$$

with the usual replacements in Eq. (46) for $\mathcal{O}_3$ and $\mathcal{O}_4$. The diagram in Fig. 9(d) is absent in the broken phase, but gets reproduced by this $\mathbf{T}_i^2 \to \mathbf{T}_i\cdot(\mathbf{T}_i+\mathbf{T}_0)$ replacement.

The divergent part of the one-loop Higgs wave function, which enters the wave-function renormalization, is the same as in the unbroken phase. The finite part will also be denoted by δR^h. Specifically, for the finite part, $R^h = 1 + \delta R^h$ is the residue of the pole in the propagator, $S \sim iR^h/(p^2 - M_h^2)$.

Next, we consider the contribution through the rescattering diagram of the terms in Eq. (45). Writing out

$$(\phi^\dagger\phi)^2 = v(h^3 + h\varphi^a\varphi^a) + \dots, \quad (54)$$

we note that diagrams involving the h^3 interaction gain a factor of 3 compared to $h\varphi^a\varphi^a$ from symmetry. We reproduce the same results as in the unbroken phase: there is no contribution from $\mathcal{O}_2$ and $\mathcal{O}_3$ and there is a relative factor of 3 between the divergent contribution for $\mathcal{O}_1$ and $\mathcal{O}_4$. The finite terms, which enter in the low-scale matching at μ_l, are given by

$$D_\lambda^{\rm fin} = -\frac{\lambda}{16\pi^2}\sum_j \eta_j^{\mathcal{O}} I_\lambda^j, \quad (55)$$

$$I_\lambda^j = 2 - \log\frac{M_j^2}{\mu_l^2} - 2\sqrt{\frac{M_h^2-4M_j^2}{M_h^2}}\tanh^{-1}\sqrt{\frac{M_h^2}{M_h^2-4M_j^2}}.$$

Here, the sum over j is over $j = h, Z, W$, with combinatorial weight $\eta_h^{\mathcal{O}} = \{3,0,0,3\}$, $\eta_W^{\mathcal{O}} = \{2,0,0,-2\}$, $\eta_Z^{\mathcal{O}} = \{1,0,0,1\}$ for $\{\mathcal{O}_1,\mathcal{O}_2,\mathcal{O}_3,\mathcal{O}_4\}$. For the anomalous dimension, mass effects are unimportant, which is why we only needed $c^{\mathcal{O}} = (\eta_h^{\mathcal{O}} + \eta_W^{\mathcal{O}} + \eta_Z^{\mathcal{O}})/2$.

The tadpole graph in Fig. 14 only attaches to h_0, and thus contributes universally to all the operators. The scalar one-point function will be denoted by Γ^h, which we use for both the finite and divergent pieces, depending on the context. Since we are working in terms of operators with one external scalar, we need to remove the VEV and include a 0-momentum propagator to attach the tadpole, leading to $\Gamma^h/(M_h^2 v)$.

Adding up all the diagrams

$$\frac{\alpha}{4\pi}\Big[\sum_i \mathbf{T}_i\cdot(\mathbf{T}_i+\mathbf{T}_0)\big(I_n^i - I_{n,\varnothing}^i\big) + \sum_{(ij)}\mathbf{T}_i\cdot\mathbf{T}_j I_s^{ij}\Big]$$
$$+ \sum_i \frac{1}{2}\delta R^i + D_\lambda + \frac{\Gamma^h}{M_h^2 v}, \quad (56)$$

where the sum over the $SU(2)$ and $U(1)$ gauge group is implicit. We can use gauge invariance of the operator, $\mathbf{T}_0 + \sum_i \mathbf{T}_i = 0$, with the action of $\mathbf{T}_h$ and $\mathbf{T}_0$ defined in Eqs. (48) and (53), to show that the Δ regulators cancel.

We will now compare the divergent terms in Eq. (56) to the result in the unbroken phase in Eq. (41) [plus the rescattering contribution in Eq. (44)]. The difference with the unbroken phase amounts to one less Higgs wavefunction renormalization, an additional tadpole contribution and no $I_F^\psi = I_F^\phi$ with $\mathbf{T}_i \cdot \mathbf{T}_0$ color structure:

$$\frac{\Gamma^h}{M_h^2 v} - \frac{1}{2}\delta R^h - \frac{\alpha C_F}{4\pi}I_F = -\delta Z_v. \quad (57)$$

This is equal to the renormalization of the VEV. Since we are now evaluating the VEV at the hard scale, this additional piece in the anomalous dimension converts $v(\mu_h) \to v(\mu_l)$, to give precisely the same result as in the unbroken computation.

C. Low-Scale Matching

The last piece of the computation is the low-scale matching at μ_l, where the W and Z are integrated out,

and one matches onto a theory with photons and gluons. For the low-scale matching we need the finite part of Eq. (56), taking into account that only the W and Z get integrated out [see Eq. (48)] and including the effect of the masses. We find that

$$\mathbf{D}\mathcal{O}_1 = vh_n\left[\left(\frac{1}{2}\delta R^h - \frac{\lambda}{16\pi^2}\sum_j \eta_j^1 I_\lambda^j + \frac{\Gamma^h}{M_h^2 v}\right)O + \mathbf{D}O\right],$$

$$\mathbf{D}\mathcal{O}_2 = \frac{vh_n}{4}\left[\frac{\alpha_W}{4\pi}\sum_i(I_s^{ih} - I_n^i + I_{n,\varnothing}^i)(\mathbf{T}_i^1 O^1 + \mathbf{T}_i^2 O^2) + \frac{\alpha_Z}{4\pi}\sum_i(I_s^{ih} - I_n^i + I_{n,\varnothing}^i)\mathbf{T}_i^Z O^3\right],$$

$$\mathbf{D}\mathcal{O}_3 = -\frac{vh_n}{2}\left[\frac{\alpha_Z}{4\pi}\sum_i(I_s^{ih} - I_n^i + I_{n,\varnothing}^i)\mathbf{T}_i^Z O\right],$$

$$\mathbf{D}\mathcal{O}_4 = -\frac{vh_n}{2}\left\{\left[\frac{\alpha_W}{4\pi}(I_n^h - I_{n,\varnothing}^h) + \frac{1}{2}\delta R^h - \frac{\lambda}{16\pi^2}\sum_j \eta_j^4 I_\lambda^j + \frac{\Gamma^h}{M_h^2 v}\right]O^3 + \frac{\alpha_W}{4\pi}\sum_i(I_s^{ih} + I_n^i - I_{n,\varnothing}^i)\frac{1}{2}i\epsilon^{ab3}\mathbf{T}_i^a O^b + \mathbf{D}O^3\right\},$$

(58)

where the gauge boson mass is M_W (M_Z) in the terms involving α_W (α_Z). The sum i runs over all the fermions in O and j runs over h, W, Z. The $\mathbf{D}$ on the right-hand side of this equation denotes the low-scale matching for the fermions. This is given in terms of the collinear and soft functions of Refs. [9, 10] by reshuffling terms between $I_n^i - I_{n,\varnothing}^i$ and I_s^{ij}, as discussed there. A consequence of this reshuffling is that

$$I_n^i - I_{n,\varnothing}^i \rightarrow \left(2\log\frac{\bar{n}_i\cdot p_i}{\mu}\log\frac{M^2}{\mu^2} - \frac{1}{2}\log^2\frac{M^2}{\mu^2} - 2\log\frac{M^2}{\mu^2} - \frac{5\pi^2}{12} + 2\right),$$

$$I_n^h - I_{n,\varnothing}^h \rightarrow \left[2\log\frac{\bar{n}_h\cdot p_h}{\mu}\log\frac{M^2}{\mu^2} - \frac{1}{2}\log^2\frac{M^2}{\mu^2} - \log\frac{M^2}{\mu^2} - \frac{5\pi^2}{12} + 1 + f_S\left(\frac{M_h^2}{M^2}, 1\right)\right],$$

$$I_s^{ih} \rightarrow -2\log\frac{-n_i\cdot n_h - i0}{2}\log\frac{M^2}{\mu^2},$$

(59)

in the above equation. For the operators $\mathcal{O}_2$ and $\mathcal{O}_3$, all the terms that do not depend on the particle i actually cancel out in the sum on i. For $\mathcal{O}_4$ a similar cancellation comes about through

$$\sum_i \frac{1}{2}i\epsilon^{ab3}\mathbf{T}_i^a O^b = -O^3.$$

(60)

The expression Eq. (58) has been written in a compact form. Gauge operators such as $\mathbf{T}_i^Z$ act differently on u and d-type quarks, since they have different $SU(2)\times U(1)$ charges. The explicit expression can be readily computed from Eq. (58) by expanding out the fermion operators in Appendix B into individual fermion components. The low-scale matching will be described in full detail in Ref. [30].

The total radiative correction can now be obtained from Eqs. (43), (44) and (58). One can run the Higgs production operator in the theory below μ_l. Since the Higgs is $SU(3)\times U(1)$ neutral, the running below μ_l is identical to that of the operator O or O^a.

D. On-Shell Gauge Bosons

The discussion so far has been for the case where the two gauge bosons in Fig. 1 are off shell, so that the EFT amplitude reduces to the local operator in Fig. 2. However, this approach can also be used for more general kinematics. If one gauge boson is off shell and the other is close to on shell, then the off-shell gauge boson can be integrated out, and the vector boson fusion amplitude reduces to a $\bar{q}qW\phi^\dagger\phi$ interaction, multiplied by the amplitude for on-shell W production (and similarly for the Z boson). The radiative correction to the $\bar{q}qW\phi^\dagger\phi$ amplitude can be computed using the methods of this paper. The on-shell W production amplitude $q \rightarrow qW$ has no large kinematic scales, and so does not contain any large electroweak logarithms. SCET does not simplify the computation of this amplitude as there is no hard scale to integrate out, and the effective field theory result is identical to the full theory computation.

If both W bosons are close to on shell, then the $WW \rightarrow H$ amplitude no longer has a large scale, and SCET simply reproduces the full theory for this amplitude. The computations of $WW \rightarrow H$ and $q \rightarrow qW$

are far simpler than those for the full vector boson fusion amplitude, since each amplitude involves only three external on-shell fields, and there are no free kinematic variables.

In Ref. [9], it was shown that even though SCET neglects M_Z^2/s power corrections, it still reproduces the full amplitude for fermion pair production to 2% accuracy even at $Q^2 = M_Z^2$. Thus using SCET for vector boson fusion, even for gauge bosons close to on shell, should still be a reliable approximation.

V. CONCLUSIONS

Electroweak radiative corrections to Higgs production via vector boson fusion were computed using SCET. The amplitude is proportional to the gauge symmetry breaking Higgs VEV, so standard resummation methods do not apply. By contrast, standard resummation methods may be used for the QCD corrections, since they receive no contribution from the Higgs sector.

In the unbroken phase of the gauge group, the VEV is treated as an external soft field. The formalism for treating scattering with both energetic collinear fields and soft fields was developed. There is a new scalar soft-collinear transition vertex, which is part of the subleading SCET Lagrangian and contributes to the amplitude. In the broken phase of the gauge theory, there are no emissions from the line corresponding to the VEV, the contribution necessary to build up collinear Wilson lines is absent too. A subtlety when switching to the broken phase of the gauge group in SCET, is that the soft field changes its power counting when it attains a VEV.

The final result is given in Eqs. (43), (44) and (58). The $\lambda\phi^4$ coupling enters the final answer and is not power suppressed. It gives a numerically significant ($\sim -10\%$) contribution to the cross-section. This is in contrast to processes such as Higgs pair production, where the $\lambda\phi^4$ interaction was subleading in the power counting, and could be neglected. Thus an accurate measurement of the vector boson fusion process might be a way of determining λ. Detailed numerical results will be presented in a future publication [30].

ACKNOWLEDGMENTS

Appendix A: SCET Feynman Integrals

One has to be careful in evaluating SCET Feynman integrals by contours. A simple example is the tadpole graph

$$I = -ig^2 C_F f_\epsilon \int \frac{d^d k}{(2\pi)^d} \frac{1}{k^2 - M^2}$$
$$= \frac{\alpha C_F}{4\pi}\left(\frac{1}{\epsilon} - \log\frac{M^2}{\mu^2} + 1\right) M^2, \qquad (A1)$$

which is nonzero. Evaluating the graph by first doing the k^+ integral by contours gives zero. The problem is that the integrand falls like $1/k^+$, so the contour at infinity does not vanish and the method of residues cannot be used for the k^+ integral. A more insidious example is the integral

$$I = -ig^2 C_F f_\epsilon \int \frac{d^d k}{(2\pi)^d} \frac{1}{k^2 - M^2}\frac{1}{k^2}$$
$$= \frac{\alpha C_F}{4\pi}\left(\frac{1}{\epsilon} - \log\frac{M^2}{\mu^2} + 1\right). \qquad (A2)$$

For large k^+, the integrand falls like $1/(k^+)^2$, so the contour at infinity does not contribute. Evaluating the k^+ integral by contours gives zero, since the two k^+ poles are on the same side of the axis for any value of k^-. The flaw in the method is that for $k^- = 0$, the integrand does not depend on k^+, so the contour integration fails at this value of k^-, and there is a $\delta(k^-)$ term that needs to be included. Regulate the integral by introducing a p^-,

$$I \to -ig^2 C_F f_\epsilon \int \frac{d^d k}{(2\pi)^d} \frac{1}{k^2 - M^2}\frac{1}{k^+(k^- + p^-) - \vec{k}_\perp^2}, \qquad (A3)$$

so that both k^+ coefficients in the denominator do not simultaneously vanish. Then one can evaluate the k^+ integral by contours, followed by the $k_\perp$ and k^- integrals, to get the correct result as $p^- \to 0$. The entire contribution to the integral arises from $-p^- \le k^- \le 0$, which gives the $\delta(k^-)$ contribution in the limit $p^- \to 0$.

Appendix B: Operator Basis

We complete Eq. (39) by listing a basis for the O and O^a, containing the fermion fields. For Higgs production through vector boson fusion, the O and O^a needed are

$$O_A = \bar{\Psi}_3\gamma^\mu T^a\Psi_1\bar{\Psi}_4\gamma_\mu T^a\Psi_2,$$
$$O_B = C_F\bar{\Psi}_3\gamma^\mu\Psi_1\bar{\Psi}_4\gamma_\mu\Psi_2,$$
$$O_A^a = \bar{\Psi}_3\gamma^\mu T^a\Psi_1\bar{\Psi}_4\gamma_\mu\Psi_2,$$
$$O_B^a = \bar{\Psi}_3\gamma^\mu\Psi_1\bar{\Psi}_4\gamma_\mu T^a\Psi_2,$$
$$O_C^a = i\epsilon^{abc}\bar{\Psi}_3\gamma^\mu T^b\Psi_1\bar{\Psi}_4\gamma_\mu T^c\Psi_2. \qquad (B1)$$

The subscripts distinguish the (possibly) different fermion fields. We use the notation $\mathcal{O}_{1A}$ for $\mathcal{O}_1$ with O_A, etc.

We now work out the action of $\mathbf{T}_i \cdot \mathbf{T}_0$, $\mathbf{T}_i \cdot \mathbf{T}_h$ and $\mathbf{T}_h \cdot \mathbf{T}_0$ for SU(2). Under $SU(2)$, the renormalization

group evolution only mixes these ten operators within the subsets $\{\mathcal{O}_{1A}, \mathcal{O}_{1B}, \mathcal{O}_{2A}, \mathcal{O}_{2B}, \mathcal{O}_{2C}\}$ and $\{\mathcal{O}_{3A}, \mathcal{O}_{3B}, \mathcal{O}_{4A}, \mathcal{O}_{4B}, \mathcal{O}_{4C}\}$. In fact, for these bases the $\mathbf{T}_i \cdot \mathbf{T}_0$, $\mathbf{T}_i \cdot \mathbf{T}_h$ and $\mathbf{T}_h \cdot \mathbf{T}_0$ have identical expressions for both subsets. Using the notation

$$\mathbf{T}_i \cdot \mathbf{T}_j \mathcal{O}_k = \sum_m \mathcal{O}_m (\mathbf{T}_i \cdot \mathbf{T}_j)_{mk}, \qquad \text{(B2)}$$

we find

$$\mathbf{T}_1 \cdot \mathbf{T}_0 = \frac{1}{4}\begin{pmatrix} 0 & 0 & 0 & 1 & 1 \\ 0 & 0 & 1 & 0 & 0 \\ 0 & 3 & -2 & 0 & 0 \\ 1 & 0 & 0 & 0 & -1 \\ 2 & 0 & 0 & -2 & -1 \end{pmatrix},$$

$$\mathbf{T}_2 \cdot \mathbf{T}_0 = \frac{1}{4}\begin{pmatrix} 0 & 0 & 1 & 0 & -1 \\ 0 & 0 & 0 & 1 & 0 \\ 1 & 0 & 0 & 0 & 1 \\ 0 & 3 & 0 & -2 & 0 \\ -2 & 0 & 2 & 0 & -1 \end{pmatrix},$$

$$\mathbf{T}_3 \cdot \mathbf{T}_0 = \frac{1}{4}\begin{pmatrix} 0 & 0 & 0 & -1 & 1 \\ 0 & 0 & -1 & 0 & 0 \\ 0 & -3 & -2 & 0 & 0 \\ -1 & 0 & 0 & 0 & 1 \\ 2 & 0 & 0 & 2 & -1 \end{pmatrix},$$

$$\mathbf{T}_4 \cdot \mathbf{T}_0 = \frac{1}{4}\begin{pmatrix} 0 & 0 & -1 & 0 & -1 \\ 0 & 0 & 0 & -1 & 0 \\ -1 & 0 & 0 & 0 & -1 \\ 0 & -3 & 0 & -2 & 0 \\ -2 & 0 & -2 & 0 & -1 \end{pmatrix},$$

$$\mathbf{T}_h \cdot \mathbf{T}_0 = \frac{1}{4}\begin{pmatrix} -3 & 0 & 0 & 0 & 0 \\ 0 & -3 & 0 & 0 & 0 \\ 0 & 0 & 1 & 0 & 0 \\ 0 & 0 & 0 & 1 & 0 \\ 0 & 0 & 0 & 0 & 1 \end{pmatrix}. \qquad \text{(B3)}$$

Here we used $C_A = N = 2$, $C_F = \frac{3}{4}$, and the $SU(2)$ group theory identities

$$T^a T^b = \frac{1}{4}\delta^{ab} + \frac{i}{2}\epsilon^{abc}t^c, \qquad \epsilon^{abc}t^a t^b = it^c, \qquad \text{(B4)}$$
$$\epsilon^{abc}\epsilon^{abd} = 2\delta^{cd}, \qquad\qquad \epsilon^{abc}\epsilon^{ade}\epsilon^{bdf} = \epsilon^{cef}.$$

The matrix expressions for $\mathbf{T}_i \cdot \mathbf{T}_h$ in this basis can be simply obtained from the above expressions for $\mathbf{T}_i \cdot \mathbf{T}_0$ by using

$$\mathbf{T}_i \cdot \mathbf{T}_h = C\, \mathbf{T}_i \cdot \mathbf{T}_0\, C,$$
$$C = \begin{pmatrix} 1 & & & & \\ & 1 & & & \\ & & -1 & & \\ & & & -1 & \\ & & & & -1 \end{pmatrix}. \qquad \text{(B5)}$$

The action of the remaining generators, as well as complete expressions for the anomalous dimension, will be given in Ref. [30].

[1] G. F. Sterman, (1995), arXiv:hep-ph/9606312.
[2] C. W. Bauer, S. Fleming, and M. E. Luke, Phys. Rev., **D63**, 014006 (2000), arXiv:hep-ph/0005275.
[3] C. W. Bauer, S. Fleming, D. Pirjol, and I. W. Stewart, Phys. Rev., **D63**, 114020 (2001), arXiv:hep-ph/0011336.
[4] C. W. Bauer and I. W. Stewart, Phys. Lett., **B516**, 134 (2001), arXiv:hep-ph/0107001.
[5] C. W. Bauer, D. Pirjol, and I. W. Stewart, Phys. Rev., **D65**, 054022 (2002), arXiv:hep-ph/0109045.
[6] J.-y. Chiu, F. Golf, R. Kelley, and A. V. Manohar, Phys. Rev. Lett., **100**, 021802 (2008), arXiv:0709.2377 [hep-ph].
[7] J.-y. Chiu, F. Golf, R. Kelley, and A. V. Manohar, Phys. Rev., **D77**, 053004 (2008), arXiv:0712.0396 [hep-ph].
[8] J.-y. Chiu, R. Kelley, and A. V. Manohar, Phys. Rev., **D78**, 073006 (2008), arXiv:0806.1240 [hep-ph].
[9] J.-y. Chiu, A. Fuhrer, R. Kelley, and A. V. Manohar, Phys. Rev., **D80**, 094013 (2009), arXiv:0909.0012 [hep-ph].
[10] J.-y. Chiu, A. Fuhrer, R. Kelley, and A. V. Manohar, Phys. Rev., **D81**, 014023 (2010), arXiv:0909.0947 [hep-ph].
[11] T. Han, G. Valencia, and S. Willenbrock, Phys. Rev. Lett., **69**, 3274 (1992), arXiv:hep-ph/9206246.
[12] T. Figy, C. Oleari, and D. Zeppenfeld, Phys. Rev., **D68**, 073005 (2003), arXiv:hep-ph/0306109.
[13] E. L. Berger and J. M. Campbell, Phys. Rev., **D70**, 073011 (2004), arXiv:hep-ph/0403194.
[14] K. Arnold et al., Comput. Phys. Commun., **180**, 1661 (2009), arXiv:0811.4559 [hep-ph].
[15] R. V. Harlander, J. Vollinga, and M. M. Weber, Phys. Rev., **D77**, 053010 (2008), arXiv:0801.3355 [hep-ph].
[16] P. Bolzoni, M. Zaro, F. Maltoni, and S.-O. Moch, (2010), arXiv:1006.2323 [hep-ph].
[17] P. Bolzoni, F. Maltoni, S.-O. Moch, and M. Zaro, Phys. Rev. Lett., **105**, 011801 (2010), arXiv:1003.4451 [hep-ph].
[18] M. Ciccolini, A. Denner, and S. Dittmaier, Phys. Rev. Lett., **99**, 161803 (2007), arXiv:0707.0381 [hep-ph].
[19] M. Ciccolini, A. Denner, and S. Dittmaier, Phys. Rev., **D77**, 013002 (2008), arXiv:0710.4749 [hep-ph].
[20] J.-y. Chiu, A. Fuhrer, A. H. Hoang, R. Kelley, and A. V. Manohar, Phys. Rev., **D79**, 053007 (2009), arXiv:0901.1332 [hep-ph].
[21] A. V. Manohar and I. W. Stewart, Phys. Rev., **D76**, 074002 (2007), arXiv:hep-ph/0605001.
[22] C. Marcantonini and I. W. Stewart, Phys. Rev., **D79**, 065028 (2009), arXiv:0809.1093 [hep-ph].

[23] J. Chay and C. Kim, Phys. Rev., **D65**, 114016 (2002), arXiv:hep-ph/0201197.

[24] M. Beneke, A. P. Chapovsky, M. Diehl, and T. Feldmann, Nucl. Phys., **B643**, 431 (2002), arXiv:hep-ph/0206152.

[25] T. Feldmann, Nucl. Phys. Proc. Suppl., **121**, 275 (2003), arXiv:hep-ph/0209239.

[26] D. Pirjol and I. W. Stewart, Phys. Rev., **D67**, 094005 (2003), arXiv:hep-ph/0211251.

[27] M. E. Luke and A. V. Manohar, Phys. Lett., **B286**, 348 (1992), arXiv:hep-ph/9205228.

[28] A. V. Manohar, T. Mehen, D. Pirjol, and I. W. Stewart, Phys. Lett., **B539**, 59 (2002), arXiv:hep-ph/0204229.

[29] A. V. Manohar, Phys. Rev., **D68**, 114019 (2003), arXiv:hep-ph/0309176.

[30] F. Siringo and G. Buccheri, (2012), arXiv:1207.1906 [hep-ph].